Radiation Physics and Chemistry 198 (2022) 110207

Contents lists available at ScienceDirect

Radiation Physics and Chemistry

journal homepage: www.elsevier.com/locate/radphyschem

Effects of manganese and terbium on the dosimetric properties of $CaSO_4$

Anderson M.B. Silva [a,*], Luiza F. Souza [b], Patrícia L. Antonio [c], Danilo O. Junot [c,d], Linda V.E. Caldas [c], Divanizia N. Souza [a]

[a] Departamento de Física, Universidade Federal de Sergipe, Marechal Rondon, S/N, 49.100-000, São Cristovão, SE, Brazil
[b] Centro de Desenvolvimento de Tecnologia Nuclear, CDTN/CNEN-MG, Av. Pres. Antônio Carlos, 6627, Belo Horizonte, Brazil
[c] Instituto de Pesquisas Energéticas e Nucleares, Comissão Nacional de Energia Nuclear, IPEN/CNEN-SP, Av. Prof. Lineu Preste, 2242, 05508-000, São Paulo, SP, Brazil
[d] Instituto de Física Armando Dias Tavares, Universidade do Estado do Rio de Janeiro UERJ, Rua São Francisco Xavier, 524, 20550-013, Rio de Janeiro, RJ, Brazil

ARTICLE INFO

Keywords:
dosimetric Properties
Structural properties
Optical properties
$CaSO_4$:Mn,Tb

ABSTRACT

In this study, a new $CaSO_4$ crystal doped with manganese and terbium is described and its potential for dosimetric applications is evaluated. Crystals were synthesized using the slow evaporation route, and were prepared in pellet form with the addition of Teflon. $CaSO_4$ was doped with manganese and terbium at a concentration of 0.1 mol% in each case. The crystalline structure and optical properties of the crystals were evaluated by X-ray diffraction, Fourier transform infrared spectroscopy and photoluminescence. The suitability of these crystals for thermoluminescent (TL) and optically stimulated luminescent (OSL) dosimetry was also investigated. The material showed adequate OSL and TL characteristics, such as a TL glow curve with two peaks at approximately 205 °C and 325 °C, an adequate OSL decay curve, good reproducibility, and linearity of the luminescent signals, when irradiated with doses of between 200 mGy and 150 Gy. Two trapping centers located at 0.77 and 1.02 eV were revealed. The heating rate dependence was also evaluated. The lowest detectable dose was investigated by the TL and OSL techniques, and the results were presented in mGy for both methods. It was also observed that co-doping with Mn and Tb contributed to a reduction in fading compared to $CaSO_4$:Mn and $CaSO_4$:Tb.

1. Introduction

The development and study of new dosimetric materials have been investigated in terms of the determination of the absorbed dose from ionizing radiation, for environmental (Bakr et al., 2020), personal monitoring (Haninger et al., 2015), clinical (Pradhan et al., 2008), accident retrospective and industrial applications (Yasmin et al., 2020; Rozaila et al., 2020; Korkmaz et al., 2019). Various synthetic and inorganic materials have also been studied in view of their potential applications in the field of luminescence, including stimulated luminescence dosimetry methodologies for thermoluminescence (TL) and optically stimulated luminescence (OSL) applications.

Calcium sulfate ($CaSO_4$) has been extensively investigated for dosimetric applications (Yamashita et al., 1971; Nambi et al., 1974; Lakshmanan, 1999; Kasa et al., 2006; Ingle et al., 2008; Nunes and Campos, 2008; Chagas et al., 2010; Junot et al., 2014, 2016). Despite its high TL sensitivity, $CaSO_4$ doped with manganese ($CaSO_4$:Mn) shows strong fading of its TL signal, which impairs its application in all dosimetric fields such as personal monitoring (Watanabe, 1951). In an attempt to overcome this limitation, terbium has been incorporated by researchers as a co-dopant in the $CaSO_4$ matrix, as recent studies have shown that the incorporation of new elements as co-dopants in this host has given rise to excellent TL properties (Junot et al., 2014, 2016; Silva et al., 2020). Other studies have reported that this material also has potential applications in the dosimetry of ionizing radiation using the OSL technique (Silva et al., 2020; Kulkarni et al., 2014; Kearfott et al., 2015; Guckan et al., 2017; Omanwar and Palan, 2018; Y ü ksel et al., 2019; Bahl et al., 2017). However, no published papers could be found related to $CaSO_4$ crystals doped with terbium and manganese for application in radiation dosimetry using the TL or OSL techniques. In this context, the aim of current research is to produce and characterize crystals of $CaSO_4$: Mn, Tb in order to develop a new material that is suitable for dosimetric applications. The crystalline structure and optical properties of these phosphors were studied using X-ray diffraction (XRD), Fourier transform infrared spectroscopy (FTIR) and photoluminescence (PL) techniques.

* Corresponding author.
E-mail address: andersonmanoel22@hotmail.com (A.M.B. Silva).

https://doi.org/10.1016/j.radphyschem.2022.110207
Received 14 May 2021; Received in revised form 21 February 2022; Accepted 1 May 2022
Available online 19 May 2022

2. Materials and methods

2.1. Sample preparation

The slow evaporation method was used to prepare $CaSO_4$:Mn,Tb. The production process was based on a mixture of calcium carbonate ($CaCO_3$) (Merck, 99%), sulfuric acid (H_2SO_4) (Vetec, 95–99%), and the precursors for the dopants. The dopant and co-dopant used were terbium oxide (Tb_4O_7) (Alfa Aesar, 99.9%) and manganese nitrate ($Mn(NO_3)_2{*}4H_2O$), at a concentration of 0.1 mol%, in a 1:1 ratio. Additional information about the experimental procedure can be found in (Junot et al., 2016; Silva et al., 2020). The resulting powder was calcined for 1 h at 600 °C. The crystalline structure and optical properties of the crystals in powder form were analyzed. To evaluate the dosimetric properties, the powder was then mixed uniformly with polytetrafluoroethylene (Teflon), in a 2:1 ratio. A uniaxial pressure of 0.5 tons was applied over 10 s to produce pellets of 40 ± 1 mg, 6 mm in diameter and approximately 1 mm thickness. Finally, the pellets were sintered at 450 °C for 1 h.

2.2. Sample characterization

XRD measurements of $CaSO_4$:Mn, Tb phosphor were performed using a Rigaku diffractometer (RINT, 2000/PC) with Cu Kα radiation of wavelength k = 0.1541 nm. The powder diffractogram was obtained in the continuous scanning mode from 20° to 80° in steps of 0.05°/min, with the X-ray tube operating at 40 kV and 30 mA. Phase identification was performed using the International Center for Diffraction Data (ICDD) PDF 00-037-1496.

Infrared (IR) absorption measurements were performed using the KBr pellet technique. The FTIR spectrum was recorded between 4000 and 400 cm^{-1} using a Prestige-21 FTIR spectrophotometer (Shimadzu, Japan). The excitation and emission spectra were obtained using a JASCO FP8600 spectrofluorometer.

The TL/OSL characteristics of $CaSO_4$:Mn, Tb samples were monitored using a Risø TL/OSL DA-20 automatic reader. The samples were irradiated with a beta source, which was coupled to the Risø system with a dose rate of 81.6 mGy/s. Except for the fading analyses, all OSL/TL measurements were carried out immediately after irradiation.

A Hoya U-34 (340 ± 40) nm filter was used in the reader for the TL/OSL measurements. To analyze the dependence on heating rate, the pellets were exposed to a range of heating rates from 1 to 10 °C/s; for all the other measurements, the heating rate was kept at 10 °C/s. Glow curve deconvolutions and TL kinetic parameters were obtained by means of OriginLab 8.0 software (OriginLab Co., USA). The TL curve was fitted using the equation for the general kinetic order presented by Chen and McKeever (1997), to determine the kinetic order (b), activation energy (E) and frequency factor (s) parameters of the TL peaks.

To assess the peaks in the TL emission curves of $CaSO_4$:Mn, Tb, the (T_m−T_{stop}) technique was applied to the samples. Each sample was first preheated to a given temperature (T_{stop}), and the average temperature of the lowest temperature peak observed (T_m) was evaluated. The T_{stop} temperature was varied in increments of 10 °C up to a final temperature of 320 °C. The samples were irradiated with a 1.66 Gy beta radiation dose, and the initial T_{stop} temperature was 120 °C. The sample was then cooled, and the complete glow curve was obtained in order to extract the value of T_m.

For the TL emission spectra measurements, a high-sensitivity spectrometer (Ocean Optics QE65 Pro) was coupled to the Risø TL/OSL reader. For the OSL readings, the samples were stimulated with blue LEDs (with emission centered at 470 nm). All measurements were performed in continuous wave mode. After each measurement, the pellets were annealed at 400 °C for 2 h, using a programmable oven, and then reused.

3. Results and discussion

3.1. Structural characterization

Fig. 1 shows the XRD pattern for $CaSO_4$:Tb, Mn powder, and it can be seen that the diffraction peaks agree with the ICDD 00-037-1496 pattern. The crystal has orthorhombic symmetry with a Bmmb space group. Its diffraction peaks and relative intensities correspond to the anhydride structure, with lattice parameters of a = 6.9933 Å, b = 7.0017 Å and c = 6.2411 Å, as reported previously (Bastani et al., 2019; Doull et al., 2014). No evidence of secondary phases or impurities was detected, indicating that the Tb^{3+} and Mn^{2+} ions were completely dissolved in the $CaSO_4$ host matrix without inducing significant changes in the crystal structure.

3.2. Fourier transform infrared spectroscopy spectra

The FTIR spectra for $CaSO_4$:Mn, Tb are shown in Fig. 2. It can be seen that there is a broad band centered at about 3440 cm^{-1}, which is assigned to the stretching vibration of the OH groups (Bezrodna et al., 2004). The band at 2970 cm^{-1} and the two low-intensity bands at 2932 and 2885 cm^{-1} result from C–H stretching (Coates Meyers, 2000).

The doublet observed at around 2350 cm^{-1} is due to CO_2 stretching, and the two bands at 2246 and 2135 cm^{-1} are related to the stretching of the carbon-carbon triple bond in alkynes (McIntosh et al., 2017; Bhadane et al., 2016). The vibrational modes of the bending of the C–H bond are also observed at 1465 and 1375 cm^{-1} (Coates Meyers, 2000). Lastly, the formation of the sulfate bond is shown in the range 1300 to 500 cm^{-1}, with peaks at 1155, 950, 679 and 613 cm^{-1} that are assigned to (SO_4) stretching and bending vibrations (Martin et al., 1987).

3.3. Photoluminescence studies

The excitation and emission spectra of $CaSO_4$:Mn, Tb phosphor are shown in Fig. 3. Upon excitation at 545 nm, the phosphor exhibits a band with a maximum at 228 nm, which is attributed to the transition from 4f to 5d in Tb^{3+} and a weak absorption band from 240 to 400 nm, corresponding to the Tb^{3+} 4f-4f transition. The emissions obtained under excitation at 228 nm consist of $4f^8 \rightarrow 4f^8$ transitions in the green and blue regions. These emissions are assigned to the $^5D_4 \rightarrow {}^7F_J$ (J = 6,5,4,3) transitions in the green region, and $^5D_3 \rightarrow {}^7F_J$ (J = 5,4,3,2) in the blue region (Li et al., 2017).

Fig. 4 shows the excitation and emission spectra (monitored at 493 and 398 nm, respectively). The excitation spectrum shows three excitation bands in the wavelength range 360–450 nm, which are related to the transitions of the Mn^{2+} ions from the ground state $^6A_1(^6S)$ to the ^4E

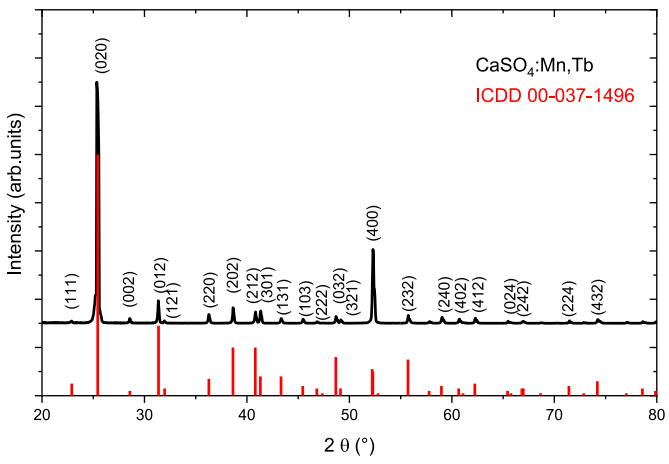

Fig. 1. Experimental X-ray diffraction results for $CaSO_4$:Mn, Tb powder, showing the crystallographic pattern and standard Bragg reflections.

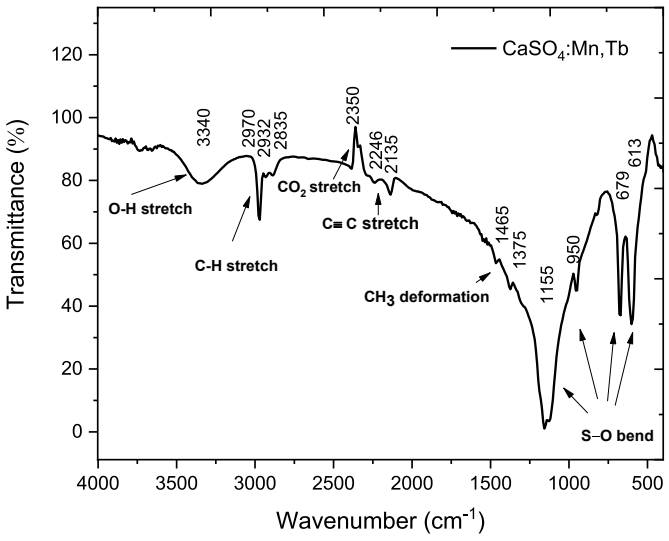

Fig. 2. FTIR spectra for $CaSO_4$:Mn,Tb.

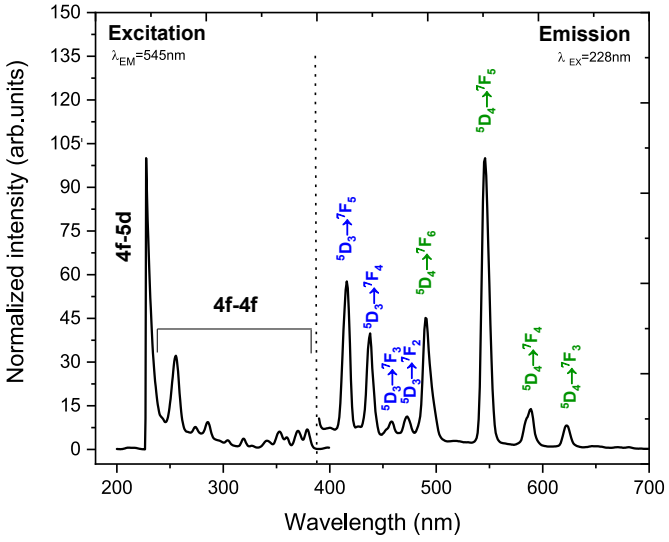

Fig. 3. Photoluminescence excitation and emission spectra for $CaSO_4$:Mn,Tb.

(^4D), $^4T_2(^4D)$ and [$^4A_1(^4G)$, $^4E(^4G)$] excited states (Hou et al., 2012). The emission obtained at 398 nm consists of two peaks, the first with higher intensity at 493 nm, and the second with lower intensity at 545 nm. These results confirm the efficiency contributions of Tb^{3+} and Mn^{2+} in $CaSO_4$. The green emission at ~500 nm is typical of divalent manganese ions, in the regular fourfold tetrahedral coordination, and corresponds to the $^4T_1 \rightarrow {}^6A_1$ transition for the Mn^{2+} ion (Luchechko et al., 2019). The values obtained in this work are similar to those reported by Zahedifar et al. (2011). The other emission observed corresponds to the $^5D_4 \rightarrow {}^7F_5$ transition for the Tb^{3+} ion (Li et al., 2017).

3.4. Dosimetric characterization

3.4.1. Thermoluminescence glow curve

Fig. 5 shows the TL glow curve for $CaSO_4$:Mn, Tb samples exposed to 1 Gy of beta radiation. The phosphor shows two dosimetric peaks at approximately 205 ° C and 325° C, as confirmed by the deconvolution of the TL glow curve. The fitting results give a good correlation coefficient ($R^2 = 0.998$) for both TL peaks.

Table 1 shows the TL parameters obtained by employing the general kinetic order fitting. The peak temperatures (T_m), maximum peak

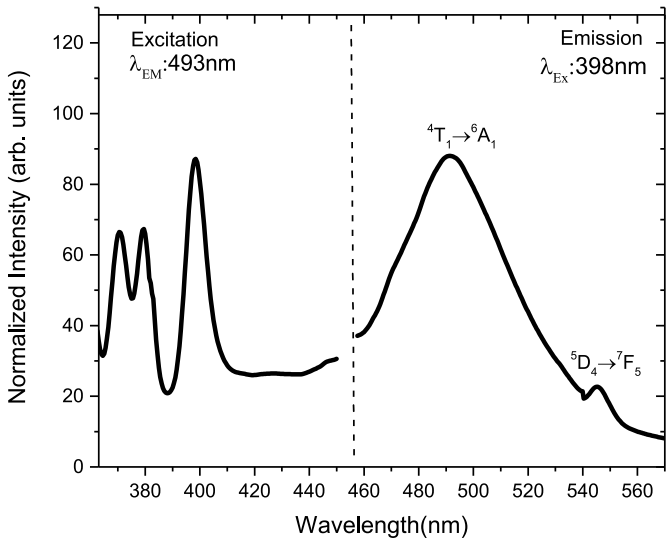

Fig. 4. Excitation and emission spectra for the $CaSO_4$:Mn, Tb sample (λ_{ex} = 493 nm, λ_{em} = 398 nm).

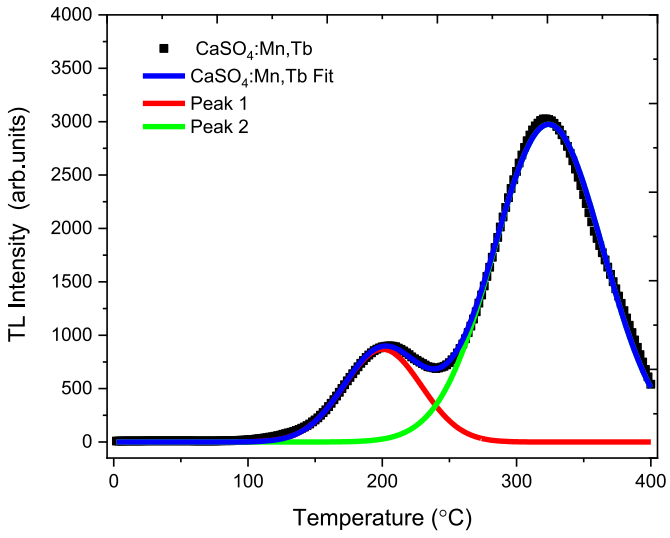

Fig. 5. TL glow curve deconvolution for $CaSO_4$:Mn,Tb, calculated using the general-order empirical expression.

Table 1
Parameters of the TL glow curve of $CaSO_4$:Mn, Tb obtained by employing the general kinetic order equation described by Chen and McKeever (1997)

$CaSO_4$: Mn,Tb	T_m (K)	I_m (arb. units)	b (kinetic order)	E (eV)	S (s^{-1})
Peak 1	476.35 ± 0.43	876.34 ± 6.05	1.41 ± 0.04	0.77 ± 0.01	1.49 × 10^9
Peak 2	597.07 ± 0.14	2973.65 ± 1.59	1.86 ± 0.01	1.02 ± 0.01	3.52 × 10^9

intensities (I_m), kinetic order value (b), the activation energies (E) and frequency factor (s) were determined. The kinetic order value (b) of the first TL peak was (1.41 ± 0.04) and the value for the second TL peak was (1.86 ± 0.01). The activation energy (E) of the first peak was (0.77 ± 0.01) eV, and the value for the second peak was (1.02 ± 0.01) eV.

3.4.2. Reproducibility, linearity and fading

In order to evaluate the reproducibility of the TL intensity of the

samples, five cycles of annealing/irradiation/reading (1 Gy from a beta source) were carried out. The variations in the TL response (area under the glow curve) were below 2.9% (Fig. 6). This means that the luminescence of these samples is reproducible.

We also carried out a homogeneity study, based on the ratio of the TL response of each pellet to the mean batch response of all pellets over the five cycles. In this analysis, the average values of the TL readings of the five pellets and their respective standard deviations were considered. The results of this homogeneity evaluation are shown in Table 2. A variation coefficient ($C.V_H\%$) of between 1.53% and 3.81% was observed; this meets the requirements of the ISO 12794:2000 (ISO 12794, 2000), which states that the $C.V_H\%$ should not exceed 15%. A comparison of these TL responses (Table 2) indicates the similarity of the TL response in all of the readings.

The TL emissions of $CaSO_4$:Mn, Tb samples irradiated with doses of between 0.169 and 149.987 Gy are shown in Fig. 7(a). In order to investigate the linearity of the TL response of this material, the areas under the emission curves were integrated and a dose-response curve was obtained (Fig. 7(b)). The TL response is linear over a very wide range of beta doses, from 0.169 to 149.987 Gy; however, beyond 149.987 Gy, the TL intensity becomes saturated. The linear adjustment confirmed a good linearity in this dose range ($R^2 = 0.997$).

The change in the relative intensity of the glow peaks with further increases in the dose and saturation is well explained by the defect interaction model (DIM) and track interaction model (TIM) (Kulkarni et al., 2020). These models make it possible to describe the linearity and saturation in the TL response based on assumptions concerning the microscopic distribution of trapped charge carriers from the absorption of energy from ionizing radiation.

At low doses, the changes in the relative intensity of the glow peaks are attributed to recombination, which occurs exclusively within the trapping entity and is unaffected by competitive centers, resulting in a linear dose response. The saturation is described as arising from the overlapping of tracks in which the defect centers are heavily occupied (Kulkarni et al., 2020; Gavhane et al., 2020).

The fading of the TL response of the samples was investigated by comparing the TL emission curves for two groups of samples, one which was obtained immediately after irradiation (1 Gy) and the other after 30 days. The two groups of samples were kept under the same environmental conditions (24 °C). A comparison of the total integrated areas of the glow curves (Fig. 8) allowed us to investigate the reduction in their

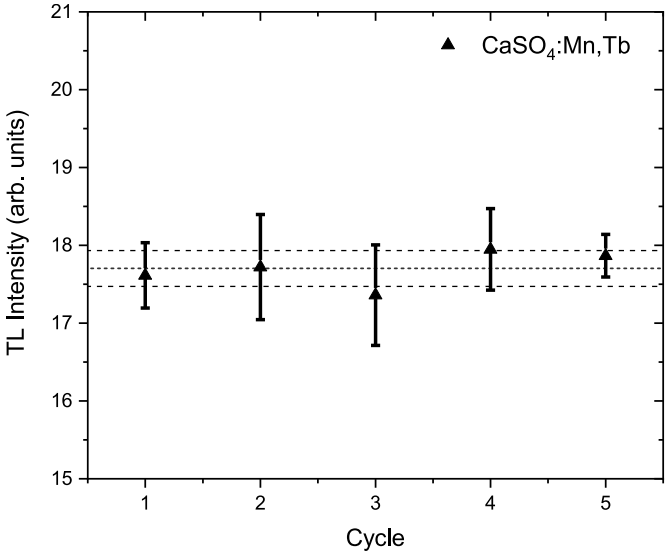

Fig. 6. TL responses (integrated area) of the $CaSO_4$:Mn, Tb samples after five cycles of the annealing/irradiation/reading procedure. The dashed lines represent the variance in the TL responses.

Table 2
Average, deviation and variation coefficient ($C.V_H\%$) of the TL response for the samples.

	Cycle 1	Cycle 2	Cycle 3	Cycle 4	Cycle 5
Average	176127.6	177204.4	173598.2	179477.5	178660.0
Deviation	4195.7	6758.0	6458.2	5243.6	2746.4
$C.V._H(\%)$	**2.38**	**3.81**	**3.72**	**2.92**	**1.53**

TL responses. The glow curve showed a reduction of 16.8% in its original value. It was also observed that TL peak above 250 °C does not fade immediately, and fades at a relatively low rate (a reduction of 10.2% in the maximum TL intensity peak), whereas the TL peak observed below 250 °C fades at a higher rate, giving a significant reduction in its intensity. This is because the energy gap between the bottom of the conduction band and the electron trap, called the 'depth trap', is smaller in the case of the second peak (Silva et al., 2020). From a dosimetric perspective, the second TL peak is more appropriate than the first, as it occurs at a higher temperature range and shows less fading after storage for four weeks. The results observed for $CaSO_4$:Mn, Tb indicate that co-doping with Mn and Tb contributed to the reduction in fading. In previous studies, fading of 60.3% over 30 days was observed for $CaSO_4$: Tb (Silva et al., 2020), and between 40% and 85% after three days of irradiation for $CaSO_4$:Mn samples (Bahl et al., 2017).

3.4.3. Heating rate dependence

To better trace the TL-related processes, TL glow curves were recorded for heating rates (β) varying from 1 to 10 °C/s. The results are illustrated in Fig. 9. As expected, the TL peaks shift to higher temperatures with an increase in the heating rate (Chen and Kirsh, 2013; Bos, 2001; Kadari and Kadri, 2015).

When the heating rate is increased from 1 to 10.0 °C/s, the TL intensity of the glow curves was found to decrease, as shown in Fig. 9(a). This observation may be explained based on the phenomenon of thermal quenching (Chen and McKeever, 1997; Kadari and Kadri, 2015).

The detailed T_m-T_{stop} dependence shown in Fig. 10 (a) confirms that there are two separate TL peaks within the temperature region examined here: one at about 206 °C, and another at 328 °C. The region above 350 °C seems to be composed of an overlap between several peaks over a broad temperature range that is limited by the parameters of the acquisition reader, with a maximum temperature of 400 °C. The first TL peak results from low-intensity traps with a well-defined energy/depth (the flat parts of the T_m-T_{stop} curve). The much more intense component is composed of a set of traps with a continuous distribution of energies (peak 2). This peak region has no clear plateau but a sharp increase at the end, indicating that the order of the glow peaks is higher than first order (Ozdemir et al., 2016); this finding is in agreement with the results presented in Section 3.4.1. Fig. 10(b) illustrates the two TL trapping levels, where the first plateau region is observed in a temperature range of 120–170°C, corresponding to a trap depth/activation energy of ~0.77 eV, and the second in the range 180–320 °C, corresponding to a trap depth/activation energy of ~1.02 eV.

3.4.4. TL emission spectra

The 3D TL emission spectra of beta-irradiated $CaSO_4$:Mn, Tb phosphors heated to each glow peak temperature are shown in Fig. 11. The emissions from the Tb^{3+} ions can be observed, with the main source of emission being the $^5D_4$ to $^7F_5$ transition at 545 nm, and less intense emissions at 378 nm ($^5D_3 \rightarrow {}^7F_6$), 412 nm ($^5D_3 \rightarrow {}^7F_5$), 435 nm ($^5D_3 \rightarrow {}^7F_4$), 453 nm ($^5D_3 \rightarrow {}^7F_3$), 470 nm ($^5D_3 \rightarrow {}^7F_2$), 488 nm ($^5D_4 \rightarrow {}^7F_6$), 586 nm ($^5D_4 \rightarrow {}^7F_4$), 619 nm ($^5D_4 \rightarrow {}^7F_3$) and 653 nm ($^5D_4 \rightarrow {}^7F_2$). Emission from Mn^{2+} ions at 494 nm ($^4T_1 \rightarrow {}^6A_1$) can also be observed. The presence of both types of emission indicates that both Mn^{2+} and Tb^{3+} ions take part in the TL process.

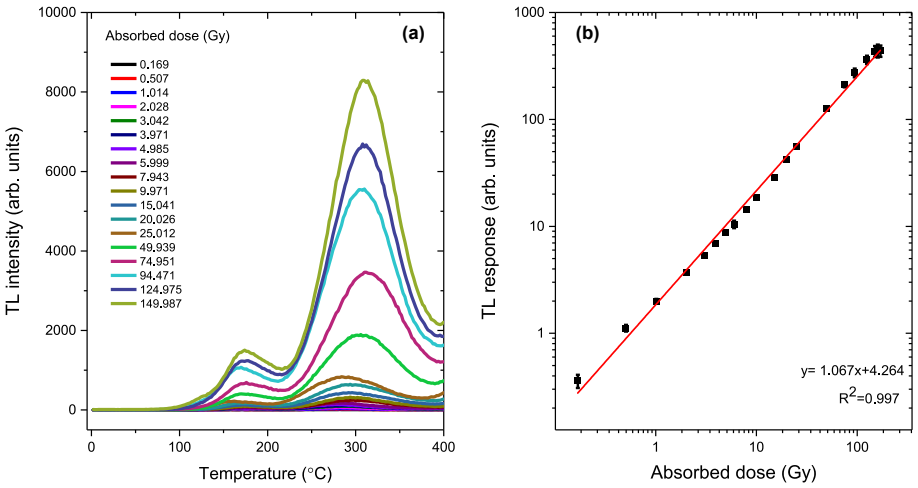

Fig. 7. (a) TL emission curves and (b) dose-response curve (integrated area) for $CaSO_4$:Mn,Tb.

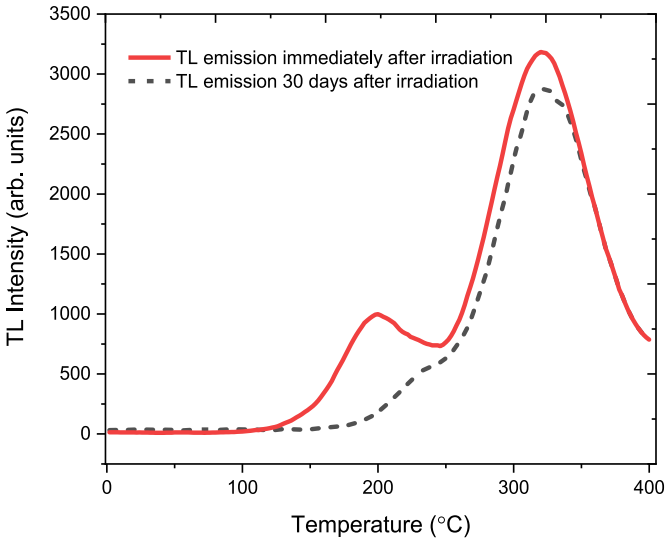

Fig. 8. TL emission for $CaSO_4$:Mn, Tb samples, read immediately after irradiation at 1 Gy ($^{90}Sr/^{90}Y$) and after 30 days.

3.4.5. OSL decay curves

Fig. 12 shows a typical OSL exponential decay curve for samples irradiated with 1 Gy, and fitted OSL decay curves. For this analysis, samples were stimulated with blue light for 40 s. The OSL signal undergoes an exponential decrease as the traps are emptied. It can therefore be presumed that the OSL response from these samples is easily stimulated at 470 nm, indicating that the traps have a high photoionization cross-section for blue LEDs.

The experimental OSL decay curves were composed of three first-order exponential decay functions, which were obtained by fitting using the following equation:

$$I_{OSL} = A_1 e^{-t/\tau_1} + A_2 e^{-t/\tau_2} + A_3 e^{-t/\tau_3}$$

where I_{OSL} is the total OSL intensity; A_1, A_2, and A_3 are constant coefficients; and τ_1, τ_2, and τ_3 are the decay constants related to the different sets of traps (Silva et al., 2020; Valen ç a et al., 2018). Table 3 shows the constant coefficients and decay constants obtained from an exponential fitting of the OSL decay curves in Fig. 12. Good agreement is observed between the fit and the experimental results.

The high value of A_1 confirms the predominance of a fast decay component in the experimental OSL decay curve; in this case, the emission of photons results in direct recombination between the electrons in the conduction band and the holes in the valence band of $CaSO_4$:Mn,Tb. The low value of $A_3 = 0.090$ indicates that the significance of the

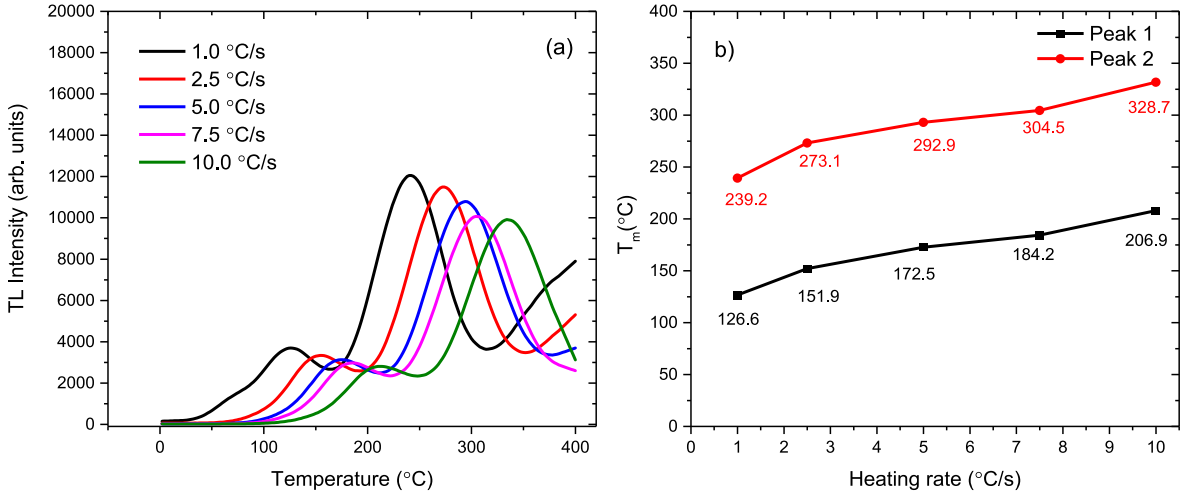

Fig. 9. (a) Dependence on heating rate of the TL glow curve for $CaSO_4$:Mn,Tb. (b) T_m dependence derived from the data presented in (a).

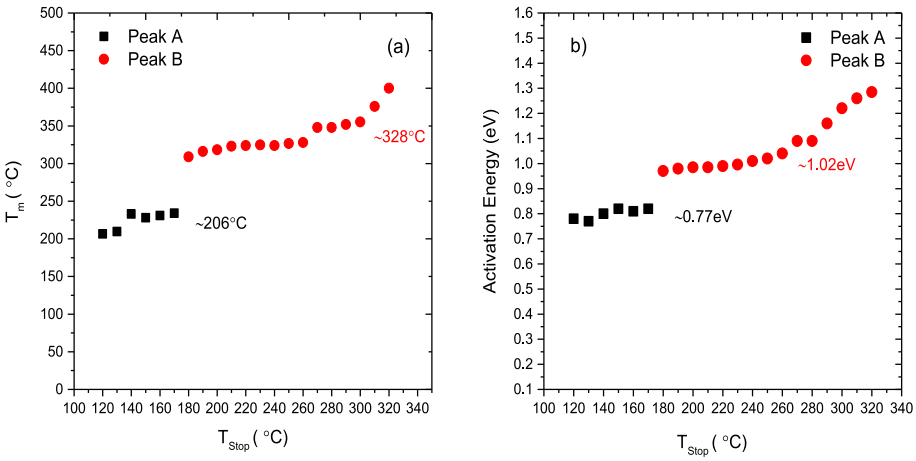

Fig. 10. (a) T_m-T_{stop} curve obtained for various preheating temperatures (T_{stop}) after irradiation of the $CaSO_4$:Mn, Tb samples with a beta radiation source. Preheating was performed using a Risø TL reader. (b) Plot of activation energy (eV) vs Tstop (°C) resulting from the T_m-T_{stop} procedure.

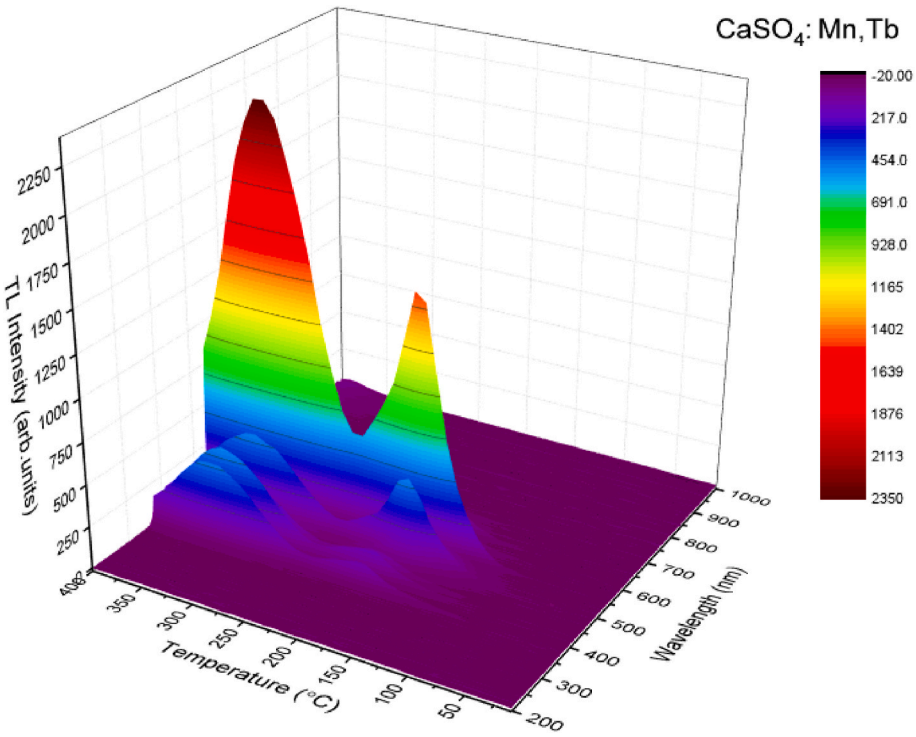

Fig. 11. TL emission spectra of $CaSO_4$:Mn, Tb samples after irradiation at 100 Gy ($^{90}Sr/^{90}Y$).

slow component ($\tau_3 = 15.186$) is minimal in the experimental OSL decay curve.

3.4.6. OSL dose response

Fig. 13(a) shows the OSL decay for $CaSO_4$:Mn, Tb samples exposed to a beta source of between 0.169 and 149.987 Gy. The OSL dose-response curve is shown in Fig. 13(b). The linear adjustments gave a high correlation coefficient ($R^2 = 0.997$) between the dose and OSL response for $CaSO_4$:Mn,Tb.

3.4.7. Lowest detectable dose

The lowest detectable dose (LDD) of the luminescent signal from the samples was calculated using the equation $LDD = (\overline{B} + \sigma_{\overline{B}})f_c$, which was proposed by Oberhofer and Scharmann (1981). In this equation, $\overline{B}$ is the average of the TL or OSL response of the non-irradiated dosimeters; $\sigma_{\overline{B}}$ is the standard deviation in the readings of non-irradiated dosimeters; and f_c is a calibration factor obtained from the inverse of the slope of the line of the TL/OSL response to the absorbed dose.

Table 4 shows the LDD values obtained. Although these values are on the same order of magnitude (in mGy), the LDD for TL is three times lower than the value achieved by the OSL technique.

3.4.8. Correlation between TL and OSL emissions

Fig. 14 shows a TL glow curve and an OSL exponential decay obtained from consecutive luminescent measurements (TL→ OSL and OSL → TL) of the $CaSO_4$:Mn, Tb samples. The previous TL measurements of the samples significantly reduced the OSL signal to background levels. It was also observed that the previous OSL reading affected the TL emission curves of the material. The traps associated with the TL peak at ~205 °C have a higher photoionization cross-section than the traps that give rise to the 325 °C peak, once their peak TL intensity has been

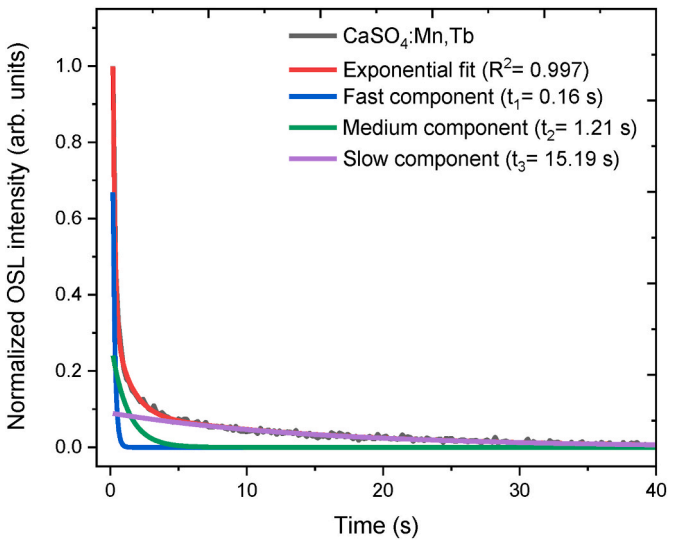

Fig. 12. OSL signal from $CaSO_4$:Mn, Tb and fitted OSL decay curves for samples irradiated with 1 Gy ($^{90}Sr+^{90}Y$).

Table 3
OSL parameters of the exponential fitted curves for the produced compound.

CW-OSL component	Coefficient A_i	Decay constant t_i (s)	Exponential fit
Fast	2.388 ± 0.075 (A_1)	0.16 ± 0.01 (t_1)	
Medium	0.283 ± 0.014 (A_2)	1.21 ± 0.06 (t_2)	R^2: 0.997
Slow	0.090 ± 0.002 (A_3)	15.19 ± 0.42 (t_3)	

reduced to 57.5% and 14.3%, respectively, even after the optical stimulation. The same behavior was reported by Silva et al. (2020) for $CaSO_4$ samples doped with terbium and silver nanoparticles.

4. Conclusions

Our X-ray diffraction analyses showed that the $CaSO_4$:Mn, Tb phosphor was efficiently synthesized by a slow evaporation route, since the XRD results indicated a single phase, which is in agreement with the ICDD 00-037-1496 pattern. The FTIR spectra showed bands in the range 1300 to 500 cm^{-1}, which are attributed to the formation of a sulfate

Table 4
LDD values for $CaSO_4$:Mn, Tb and their uncertainties for the TL and OSL techniques.

Luminescence technique	$\overline{B}$ (arb. units)	$\sigma_{\overline{B}}$ (arb. units)	f_c (mGy/ arb. units)	LDD (mGy)
TL	1781.00	188.75	0.0057	**13.51 ± 0.02**
OSL	4279.00	87.22	0.0085	**38.89 ± 0.03**

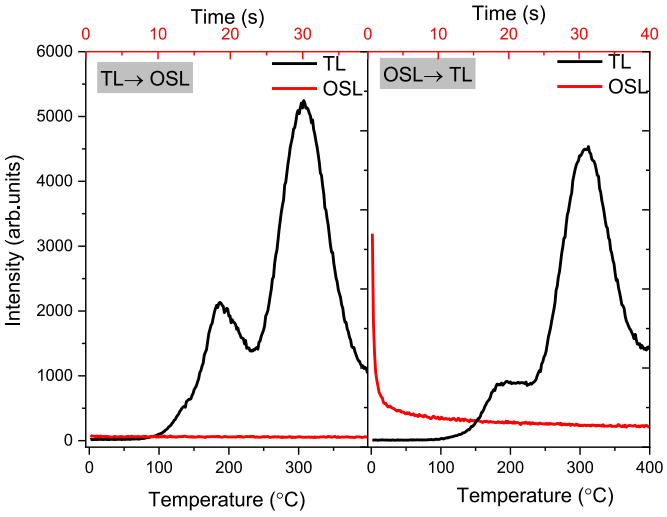

Fig. 14. Correlation between TL and OSL emissions from the $CaSO_4$:Mn, Tb samples.

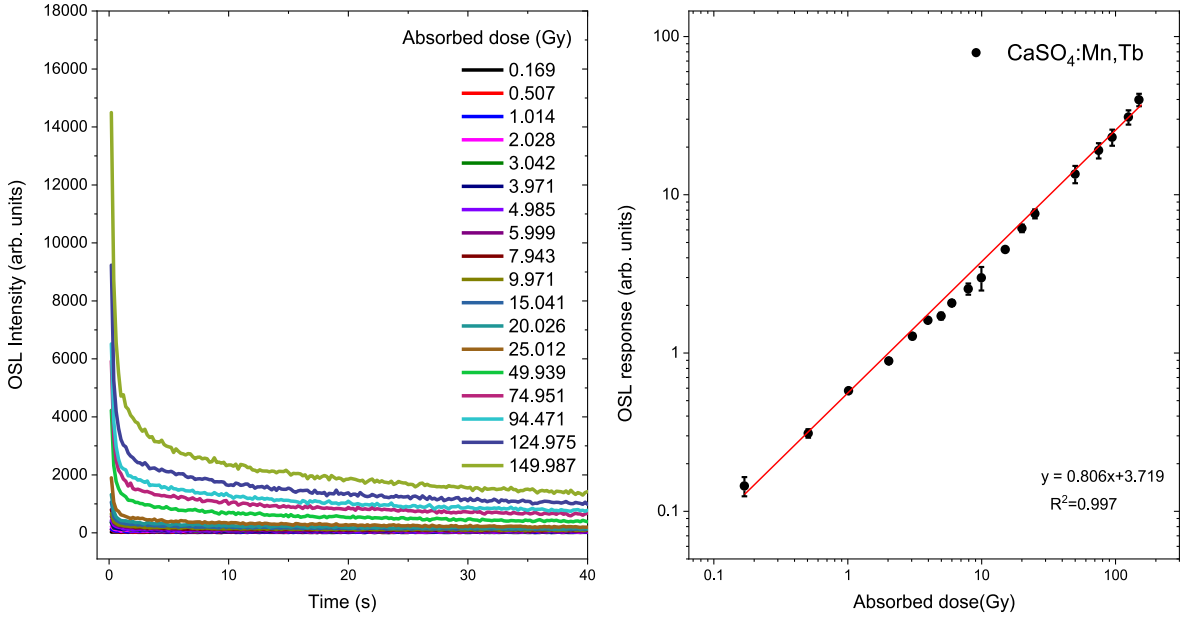

Fig. 13. (a) OSL response from the samples of $CaSO_4$:Mn, Tb and (b) as a function of the absorbed dose of beta radiation ($^{90}Sr/^{90}Y$).

bond in the samples. The other vibrational bands observed in the spectra are attributed to water vapor at 3440 cm^{-1}, atmospheric CO_2 at 2350 cm^{-1}, five hydrocarbons and two carbon-carbon triple bonds. The results for the PL and TL emission spectra confirmed the presence of Tb^{3+} and Mn^{2+} ions in the crystal matrix. The TL emission glow curves for the $CaSO_4$:Mn, Tb samples showed two peaks centered around 205 °C and 325 °C. Two trapping centers located at 0.77 and 1.02 eV were revealed. The order of kinetics was found to be between one and two, indicating the existence of a general order of kinetics in the TL process. The samples showed a typical exponential OSL decay curve with the predominance of a fast decay component, indicating that the traps have a high photoionization cross-section for blue LEDs. All samples presented properties useful for dosimetric purposes, such as linearity, reproducibility, lowest detectable doses for the OSL and TL signals, on the order of mGy, and the TL fading was 16.8% over 30 days. From these results, we can conclude that $CaSO_4$:Mn, Tb has better dosimetric properties than $CaSO_4$:Mn and $CaSO_4$:Tb.

CRediT authorship contribution statement

Anderson M.B. Silva: Conceptualization, Methodology, Investigation, Writing - original draft. **Luiza F. Souza:** Visualization, Investigation. **Patrícia L. Antonio:** Visualization, Investigation. **Danilo O. Junot:** Data curation, Investigation, Writing - review & editing. **Linda V.E. Caldas:** Conceptualization, Visualization, Resources. **Divanizia N. Souza:** Supervision, Resources, Writing - original draft, Project administration.

Declaration of competing interest

The authors declare that they have no known competing financial interests or personal relationships that could have appeared to influence the work reported in this paper.

Acknowledgments

The authors thank the Brazilian agencies Comissão Nacional de Energia Nuclear (CNEN), Coordenação de Aperfeiçoamento de Pessoal de Nível Superior - CAPES (Project 88881.157892/2017–01), Conselho Nacional de Desenvolvimento Científico e Tecnológico - CNPq (Projects: 427010/2016–0, 308090/2016–0, 151945/2019–5, 301335/2016–8, 160306/2019–1 and 466512/2018–5) and Fundação de Amparo a Pesquisa do Estado de São Paulo – FAPESP (Project 2018/05982), Brazil.

References

Bahl, S., Kumar, V., Bihari, R.R., Kumar, P., 2017. Investigations of OSL properties ofCaSO $_4$:Mn phosphor exposed to gamma and beta radiations. J. Lumin. 181, 36–43. https://doi.org/10.1016/j.jlumin.2016.09.004.

Bakr, M., Portakal Ucar, Z.G., Yuksel, M., Kaynar, U.H., Ayvacikli, M., Benourdja, S., Canimoglu, A., Topaksu, M., Hammoudeh, A., Can, N., 2020. Thermoluminescence properties of beta particle irradiated $Ca_3Al_2O_6$ phosphor relative to environmental dosimetry. J. Lumin. 227, 117565 https://doi.org/10.1016/j.jlumin.2020.117565.

Bastani, S., Oliveira, L.C., Yukihara, E.G., 2019. Development and characterization of lanthanide-doped $CaSO_4$ for temperature sensing applications. Opt. Mater. 92, 273–283. https://doi.org/10.1016/j.optmat.2019.04.022.

Bezrodna, T., Puchkovska, G., Shymanovska, V., Baran, J., Ratajczak, H., 2004. IR-analysis of H-bonded H_2O on the pure TiO_2 surface. J. Mol. Struct. 700, 175–181. https://doi.org/10.1016/j.molstruc.2003.12.057.

Bhadane, M.S., Mandlik, N., Patil, B.J., Dahiwale, S.S., Sature, K.R., Bhoraskar, V.N., Dhole, S.D., 2016. $CaSO_4$:Dy microphosphor for thermal neutron dosimetry. J. Lumin. 170, 226–230. https://doi.org/10.1016/j.jlumin.2015.10.025.

Bos, A., 2001. High sensitivity thermoluminescence dosimetry. Nucl. Instrum. Methods Phys. Res. B. 184, 3–28. https://doi.org/10.1016/S0168-583X(01)00717-0.

Chagas, M.A.P., Nunes, M.G., Campos, L.L., Souza, D.N., 2010. TL properties of anhydrous $CaSO_4$:Tm improvement. Radiat. Meas. 45, 550–552. https://doi.org/10.1016/j.radmeas.2010.01.025.

Chen, R., Kirsh, Y., 2013. The Analysis of Thermally Stimulated Processes. Pergamon Press, Oxford.

Chen, R., McKeever, S.W.S., 1997. Theory of Thermoluminescence and Related Phenomena. World Scientific, New Jersey.

Coates, J., 2000. Interpretation of infrared spectra, A practical approach. In: Meyers, R.A. (Ed.), Encyclopedia of Analytical Chemistry. J. Wiley, Chichester, U.K., pp. 10821–10822. https://doi.org/10.1002/9780470027318.a5606

Doull, B.A., Oliveira, L.C., Wang, D.Y., Milliken, E.D., Yukihara, E.G., 2014. Thermoluminescent properties of lithium borate, magnesium borate and calcium sulfate developed for temperature sensing. J. Lumin. 146, 408–417. https://doi.org/10.1016/j.jlumin.2013.10.022.

Gavhane, K.H., Bhadane, M.S., Bhoir, A.S., Kulkarni, P.P., Patil, B.J., Bhoraskar, V.N., Dhole, S.D., Dahiwale, S.S., 2020. T_m-T_{stop} analysis and dosimetric properties of Ce doped BaB_4O_7 phosphor. J. Alloys Compd. 817, 152805 https://doi.org/10.1016/j.jallcom.2019.152805.

Guckan, V., Altunal, V., Nur, N., Depci, T., Ozdemir, A., Kurt, K., Yu, Y., Yegingil, I., Yegingil, Z., 2017. Studying CaSO $_4$:Eu as an OSL phosphor. Nucl. Instrum. Methods Phys. Res. B. 407, 145–154. https://doi.org/10.1016/j.nimb.2017.06.010.

Haninger, T., Hödlmoser, H., Figel, M., König-Meier, D., Henniger, J., Sommer, M., Jahn, A., Ledtermann, G., Eßer, R., 2015. Properties of the BeOSL dosimetry system in the framework of a large-scale personal monitoring service. Radiat. Protect. Dosim. 170, 269–273. https://doi.org/10.1093/rpd/ncv425.

Hou, D., Liu, C., Kuang, X., Liang, H., 2012. Enhanced emission of Mn^{2+} via Ce^{3+}→Mn^{2+} energy transfer in α-$Sr_2P_2O_7$. Opt Express 20, 28969–28980. https://doi.org/10.1364/OE.20.028969.

Ingle, N.B., Omanwar, S.K., Muthal, P.L., Dhopte, S.M., Kondawar, V.K., Gundurao, T.K., Moharil, S.V., 2008. Synthesis of CaSO $_4$:Dy, $CaSO_4$:Eu^{3+} and $CaSO_4$:Eu^{2+}phosphors. radiat. Meas. 43, 1191–1197. https://doi.org/10.1016/j.radmeas.2008.03.005.

ISO 12794, 2000. Nuclear Energy–Radiation Protection–Individual Thermoluminescence Dosemeters for Extremities and Eyes. International Organization for Standardization, Geneva.

Junot, D.O., Couto dos Santos, M.A., Antonio, P.L., Caldas, L.V.E., Souza, D.N., 2014. Feasibility study of CaSO $_4$:Eu, $CaSO_4$:Eu,Ag and $CaSO_4$:Eu,Ag(NP) asthermoluminescent dosimeters. Radiat. Meas. 71, 99–103. https://doi.org/10.1016/j.radmeas.2014.05.022.

Junot, D.O., Barros, J.P., Caldas, L.V.E., Souza, D.N., 2016. Thermoluminescent analysis ofCaSO $_4$:Tb,Eu crystal powder for dosimetric purposes. Radiat. Meas. 90, 228–232. https://doi.org/10.1016/j.radmeas.2016.01.020.

Kadari, A., Kadri, D., 2015. New numerical model for thermal quenching mechanism in quartz based on two-stage thermal stimulation of thermoluminescence model. Arab. J. Chem. 8, 798–802. https://doi.org/10.1016/j.arabjc.2013.05.027.

Kasa, I., Chobola, R., Mell, P., Szakcacs, S., Kerekes, A., 2006. Preparation and investigation of thermoluminescence properties of $CaSO_4$:Tm,Cu, Radiat. Prot. Dosim. 123, 32–35. https://doi.org/10.1093/rpd/ncl088.

Kearfott, K.J., West, W.G., Rafique, M., 2015. The optically stimulated luminescence (OSL) properties of LiF:Mg,Ti, $Li_2B_4O_7$:Cu, $CaSO_4$:Tm, and CaF_2:Mn thermoluminescent (TL) materials. Appl. Radiat. Isot. 99, 155–161. https://doi.org/10.1016/j.apradiso.2015.03.004.

Korkmaz, G., Dilaver, M., Polat, M., 2019. ESR investigation on the potential use of potassium citrate as a dosimeter material. Appl. Radiat. Isot. 153, 108828 https://doi.org/10.1016/j.apradiso.2019.108828.

Kulkarni, M.S., Patil, R.R., Patle, A., Rawat, N.S., Ratna, P., Bhatt, B.C., Moharil, S.V., 2014. Optically stimulated luminescence from CaSO $_4$:Eu - preliminary results. Radiat. Meas. 71, 95–98. https://doi.org/10.1016/j.radmeas.2014.02.015.

Kulkarni, P.P., Gavhane, K.H., Bhadane, M.S., Bhoraskar, V.N., Dahiwale, S.S., Dhole, S. D., 2020. Investigation of the photoluminescence and novel thermoluminescence dosimetric properties of $NaGdF_4$: Tb^{3+} phosphors. Mater. Adv. 1, 1113–1124. https://doi.org/10.1039/D0MA00247J.

Lakshmanan, A.R., 1999. Photoluminescence and thermoestimulated luminescenceprocesses in rare-earth-doped CaSO $_4$ phosphors. Prog. Mater. Sci. 44, 1–187.

Li, M., Wang, L., Ran, W., Deng, Z., Shi, J., Ren, C., 2017. Tunable luminescence inSr2MgSi2O7: Tb^{3+}, Eu^{3+} phosphors based on energy transfer. Materials 10, 227. https://doi.org/10.3390/ma10030227.

Luchechko, A., Zhydachevskyy, Y., Ubizskii, S., Kravets, O., Popov, A.I., Rogulis, U., Suchocki, A., 2019. Afterglow, TL and OSL properties of Mn $^{2+}$-doped $ZnGa_2O_4$ phosphor. Sci. Rep. 9, 1–8. https://doi.org/10.1038/s41598-019-45869-7.

Martin, M.A., Childers, J.W., Palmer, R.A., 1987. Fourier transform infrared photoacoustic spectroscopy characterization of sulfur-oxygen species resulting from the reaction of SO_2 with CaO and $CaCO_3$. Appl. Spectrosc. 41, 120–126.

McIntosh, I.M., Nichols, A.R., Tani, K., Llewellin, E.W., 2017. Accounting for the species-dependence of the 3500 cm^{-1} H_2Ot infrared molar absorptivity coefficient: implications for hydrated volcanic glasses. Am. Mineral. 102, 1677–1689. https://doi.org/10.2138/am-2017-5952CCBY.

Nambi, K.S.V., Bapat, V.N., Ganguly, A.K., 1974. Thermoluminescence of $CaSO_4$ dopedwith rare earths. J. Phys. C Solid State Phys. 7, 4403–4415. https://doi.org/10.1088/0022-3719/7/23/027.

Nunes, M.G., Campos, L.L., 2008. Study of $CaSO_4$:Dy and LiF:Mg,Ti detectors TL response to electron radiation using a SW Solid Water phantom. Radiat. Meas. 43, 459–462. https://doi.org/10.1016/j.radmeas.2007.11.008.

Oberhofer, M., Scharmann, A., 1981. Applied Thermoluminescence Dosimetry. CRCPress, Ispra.

Omanwar, S.K., Palan, C.B., 2018. Synthesis and preliminary OSL studies of Ce3þ activated calcium sulfate ($CaSO_4$) for radiation dosimetry. J. Mater. Sci. Mater. Electron. 29, 7388–7392. https://doi.org/10.1007/s10854-018-8728-6.

Ozdemir, A., Yegingil, Z., Nur, N., Kurt, K., Tuken, T., Depci, T., Tansug, G., Altunal, V., Guckan, V., Sigircik, G., Yu, Y., Karatasli, M., Dolek, Y., 2016. Thermoluminescence study of Mn doped lithium tetraborate powder and pellet samples synthesized by solution combustion synthesis. J. Lumin. 173, 149–158. https://doi.org/10.1016/j.jlumin.2016.01.013.

Pradhan, A.S., Lee, J.I., Kim, J.L., 2008. Recent developments of optically stimulated luminescence materials and techniques for radiation dosimetry and clinical applications. J. Med. Phys. 33, 85–99. https://doi.org/10.4103/0971-6203.42748.

M. U Rozaila, Z.S., Khandaker, M.U., binti Wahib, N., bin Abdul Jilani, M.K.H., Sani, M.S. A., Bradley, D.A., 2020. Thermoluminescence characterization of smartphone screen for retrospective accident dosimetry. Radiat. Phys. Chem. 167, 108297. https://doi.org/10.1016/j.radphyschem.2019.04.047.

Silva, A.M.B., Junot, D.O., Caldas, L.V.E., Souza, D.N., 2020. Structural, optical and dosimetric characterization of $CaSO_4$:Tb, $CaSO_4$:Tb, Ag and $CaSO_4$:Tb,Ag(NP). J. Lumin. 224, 117286 https://doi.org/10.1016/j.jlumin.2020.117286.

Valença, J.V.B., Silva, A.C.A., Dantas, N.O., Caldas, L.V.E., d'Errico, F., Souza, S.O., 2018. Optically stimulated luminescence of the 20Li $_2CO_3$ – (X)K_2CO_3 – (80 -X)B2O3 glass system. J. Lumin. 200, 248–253. https://doi.org/10.1016/j.jlumin.2018.03.060.

Watanabe, K., 1951. Properties of $CaSO_4$:Mn phosphor under vacuum ultraviolet excitation. Phys. Rev. 83, 785–791. https://doi.org/10.1103/PhysRev.83.78.

Yüksel, M., Dogan, T., Portakal, Z.G., Topaksu, M., 2019. Synthesis and luminescencecharacterization of microcrystalline Nd-doped calcium sulfate. Appl. Radiat. Isot. 148, 197–203. https://doi.org/10.1016/j.apradiso.2019.04.005.

Yamashita, T., Nada, N., Onishi, H., Kitamura, S., 1971. Calcium sulfate activated bythulium or dysprosium for thermoluminescence dosimetry. Health Phys. 21, 295–300.

Yasmin, S., Khandaker, M.U., Rozaila, Z.S., Rashid, M.A., Bradley, D.A., Sani, S.A., 2020. Thermoluminescence features of commercial glass and retrospective accident dosimetry. Radiat. Phys. Chem. 168, 108528 https://doi.org/10.1016/j.radphyschem.2019.108528.

Zahedifar, M., Mehrabi, M., Harooni, S., 2011. Synthesis of $CaSO_4$:Mn nanosheets with high thermoluminescence sensitivity. Appl. Radiat. Isot. 69, 1002–1006. https://doi.org/10.1016/j.apradiso.2011.01.036.